Hexa-*peri*-hexabenzocoronene with Different Acceptor Units for Tuning Optoelectronic Properties

Ashok Keerthi,[a] Ian Cheng-Yi Hou,[a] Tomasz Marszalek,[a] Wojciech Pisula,[a, b] Martin Baumgarten,[a] and Akimitsu Narita*[a]

Abstract: Hexa-*peri*-hexabenzocoronene (HBC)-based donor-acceptor dyads were synthesized with three different acceptor units, through two pathways: 1) "pre-functionalization" of monobromo-substituted hexaphenylbenzene prior to the cyclodehydrogenation; and 2) "post-functionalization" of monobromo-substituted HBC after the cyclodehydrogenation. The HBC-acceptor dyads demonstrated varying degrees of intramolecular charge-transfer interactions, depending on the attached acceptor units, which allowed tuning of their photophysical and optoelectronic properties, including the energy gaps. The two synthetic pathways described here can be complementary and potentially be applied for the synthesis of nanographene-acceptor dyads with larger aromatic cores, including one-dimensionally extended graphene nanoribbons.

Large polycyclic aromatic hydrocarbons (PAHs), as represented by hexa-*peri*-hexabenzocoronene (HBC), have been attracting a renewed attention as nanographene molecules, having defined nanoscale graphene structures with distinct optical and electronic properties.[1] Such nanographene molecules bear high potential not only for applications in electronic and optoelectronic devices as organic semiconductors or structurally defined graphene quantum dots,[1-2] but also as models for studying chemical functionalization and structural modification of graphene and graphene nanoribbons (GNRs).[1a, 3] A series of nanographene molecules with different structures, e.g., size and edge configuration, as well as heteroatom doping, have thus far been synthesized, demonstrating the possibility of fine-tuning their photophysical and optoelectronic properties through the structural modulation.[1a, 1b, 4] Nevertheless, the peripheral functionalization of such nanographene molecules with different functional groups has been relatively underdeveloped, despite the vast opportunities of bestowing new functions on them as well as modulating their properties without changing the aromatic core structures.[5] In particular, nanographene molecules coupled with acceptor units are of great interest for lowering their energy gaps through charge-transfer interactions, although only a few such examples are known in the literature.[6]

To this end we have selected HBC as a model system for exploring the functionalization of nanographene molecules with different acceptor units. HBC derivatives have gained great interest as organic functional materials with phase-forming behavior, serving as donor materials in organic photovoltaics (OPV)[6e, 7] as well as p-type semiconductors in organic field-effect transistors (OFETs).[8] Herein we report syntheses of three HBC-acceptor dyads (**HBC-A**) bearing different acceptor units, i.e., 9,10-anthraquinone (**AQ**),[9] naphthalene-1,8-dicarboximide (**NMI**),[10] and perylene-3,4-dicarboximide (**PMI**)[11] (Figure 1). The three HBC-acceptor dyads demonstrate varied photophysical and optoelectronic properties and, depending on the acceptor unit, allowed for a fine control of their optical properties and energy gaps.

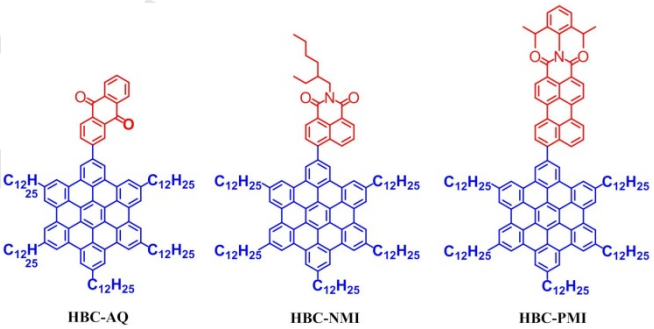

Figure 1. Chemical structures of **HBC-AQ**, **-NMI**, and **-PMI**.

The synthesis of HBC-acceptor dyads started from monobromo-substituted hexaphenylbenzene derivative **HPB-Br**[5i] and two synthetic routes were investigated in comparison: 1) "pre-functionalization" of **HPB-Br** with an acceptor unit (**A**) through a Suzuki coupling to obtain **HPB-A**, followed by oxidative cyclodehydrogenation to afford **HBC-A** (Route I, Scheme 1); 2) cyclodehydrogenation of **HPB-Br** to monobromo-substituted HBC derivative **HBC-Br**,[5i] followed by "post-functionalization" to provide **HBC-A** (Route II, Scheme 1). The pre-functionalization protocol enables facile and complete purification of the soluble, functionalized precursor **HPB-A**, although the acceptor unit might compromise the efficiency of the cyclodehydrogenation, and/or be unstable under the reaction conditions. On the other hand, the post-functionalization protocol can ensure the completion of the cyclodehydrogenation, i.e., from **HPB-Br** to **HBC-Br**, and is more straightforward for preparing various **HBC-A** with different acceptor units, whereas the separation of the resulting **HBC-A** from debrominated byproducts could be difficult, depending on their solubility. Thus, these two protocols can be complementary to each other and are worthwhile studying in comparison.

First, the synthesis was carried out through the pre-functionalization route: **HPB-Br** was coupled with boronic esters of the acceptor units, namely, 2-(4,4,5,5-tetramethyl-1,3,2-dioxaborolan-2-yl)anthracene-9,10-dione (**AQ-boro**), N-(2-

[a] Dr. A. Keerthi, I. C.-Y. Hou, Dr. T. Marszalek, Prof. Dr. W. Pisula, Prof. Dr. M. Baumgarten, Dr. A. Narita
Max Planck Institute for Polymer Research
Ackermannweg 10, 55128 Mainz (Germany)
E-mail: narita@mpip-mainz.mpg.de
[b] Prof. Dr. W. Pisula
Department of Molecular Physics, Faculty of Chemistry
Lodz University of Technology
Zeromskiego 116, 90-924 Lodz (Poland)

Supporting information for this article is given via a link at the end of the document.

ethylhexyl)-4-(4,4,5,5-tetramethyl-1,3,2-dioxaborolan-2-yl)naphthalene-1,8-dicarboximide (**NMI-boro**), and N-(2,6-di*iso*propylphenyl)-9-(4,4,5,5-tetramethyl-1,3,2-dioxaborolan-2-yl)perylene-3,4-dicarboximide (**PMI-boro**)[12] via the Suzuki coupling to obtain **HPB-AQ**, **-NMI**, and **-PMI**, respectively (Scheme 1). Subsequently, the oxidative cyclodehydrogenation of these precursors was carried out using $FeCl_3$ in dichloromethane and nitromethane at room temperature, providing **HBC-AQ**, **-NMI**, and **-PMI**, respectively. The products were highly soluble in common organic solvents such as dichloromethane (DCM), toluene, tetrahydrofuran (THF), and ethyl acetate, which allowed for purification by silica gel column chromatography and comprehensive characterizations in solution. Structural proof was thus obtained by ^{1}H and ^{13}C NMR as well as matrix-assisted laser desorption/ionization time-of-flight (MALDI-TOF) mass spectrometry (MS) analyses (see SI), indicating that all three acceptor units did not hinder the complete cyclodehydrogenation. Nevertheless, MALDI-TOF MS analysis displayed relatively intense peaks of chlorinated byproducts for **HBC-NMI** and **-PMI**, in comparison to **HBC-AQ**, which could not be removed by the silica gel column chromatography (see Figures S17–S19). These characterizations also confirmed that no extra C-C bond was formed between the HBC core and the acceptor units during the cyclodehydrogenation, which would make a five-membered ring particularly in the cases of **HBC-NMI** and **-PMI** (Figure S1).

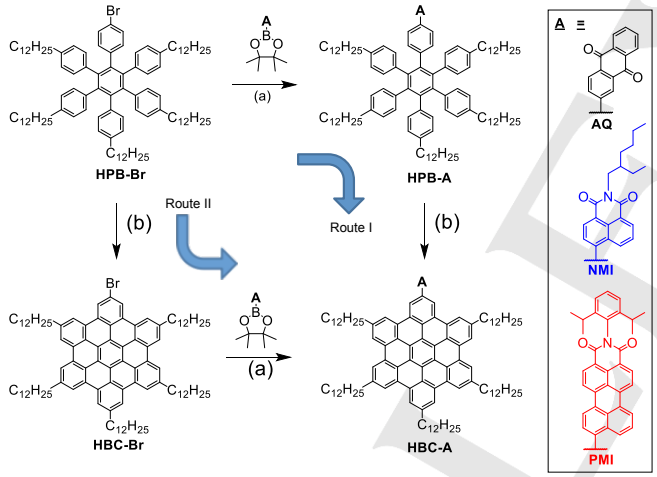

Scheme 1. Scheme Caption Synthetic routes towards HBC-acceptor dyads; a) toluene/ethanol/2 M K_2CO_3, 90 °C, 16 h; pre-functionalization: **HPB-AQ**: 74%; **HPB-NMI**: 90%; **HPB-PMI**: 54%; post-functionalization: **HBC-AQ**: 79%; **HBC-NMI**: 94%; **HBC-PMI**: 81% b) $FeCl_3$, nitromethane, dichloromethane, rt, 1 h; post-functionalization: **HBC-Br**: 83%; pre-functionalization: **HBC-AQ**: 46%; **HBC-NMI**: 91%; **HBC-PMI**: 32%.

Next, the second, post-functionalization route was applied for the syntheses of **HBC-AQ**, **-NMI**, and **-PMI**, which was expected to suppress the undesired chlorinated byproducts. **HPB-Br** was first subjected to the cyclodehydrogenation to obtain **HBC-Br**,[5i] and then to Suzuki coupling with **AQ-boro**, **NMI-boro**, and **PMI-boro** to afford **HBC-AQ**, **-NMI**, and **-PMI**, respectively (Scheme 1). The MALDI-TOF MS analyses of thus obtained **HBC-NMI** and **-PMI** samples showed significantly smaller signals from the chlorinated byproducts. Although the relative intensities in the MALDI-TOF MS analysis do not correspond to the actual ratios between different chemical species, the obvious suppression of the byproduct signals under the same measurement condition indicated the superiority of the post-functionalization route for the preparation of soluble HBC-acceptor dyads. On the other hand, the pre-functionalization route can be useful for HBC derivatives with limited solubility, which cannot be separated from debrominated byproducts through column chromatography although the cyclodehydrogenation conditions need to be carefully optimized to suppress the chlorination. It should be noted that the UV-Vis absorption and emission spectra of the HBC-acceptor dyads prepared by the pre- and post-functionalization methods were almost identical (Figures S8–10), showing that the chlorinated byproducts detected by MALDI-TOF MS had negligible influences on the optical properties of **HBC-AQ**, **-NMI**, and **-PMI**. These results indicated that both pre- and post-functionalization routes can be complementarily employed for the synthesis of different HBC-acceptor dyads, and eventually also applied for coupling larger nanographene molecules and GNRs with acceptor units.

The optical and electrochemical properties of the three HBC-acceptor dyads were investigated in comparison. UV-Vis absorption spectra of **HBC-AQ**, **-NMI**, and **-PMI** all showed the ß-band of the HBC core at ~360 nm along with the p-band at ~390 nm (Figure 2A).[13] A broad red-shifted band observed for **HBC-AQ** at 400–520 nm and for **HBC-NMI** at 400–460 nm could presumably be assigned to the intramolecular charge-transfer (CT) interactions between donor and acceptor units, although it was difficult to confirm its dependence on the polarity of the solvent[6a] due to the small absorbance (Figure S6). It should be noted that these broad bands also overlap with the α-band of the HBC core, which nevertheless does not extend over 425 nm (Figure 2A).[13] On the other hand, no red-shifted absorption band was visible in the absorption spectrum of **HBC-PMI**, compared to the absorption of the **PMI** unit itself,[11] suggesting the absence of the ground-state CT.

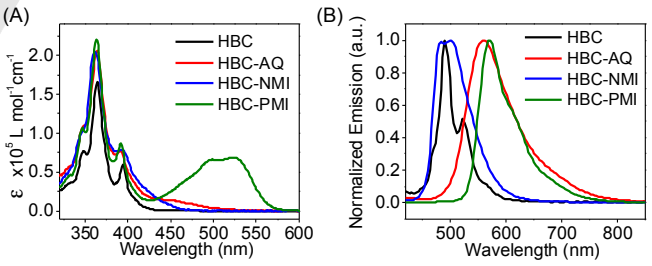

Figure 2. (A) Absorption and (B) emission spectra of the HBC-acceptor dyads in comparison with pristine HBC bearing six dodecyl chains, recorded in toluene solutions at a concentration of 10^{-5} mol/L. Excitation wavelength in the photoluminescence spectroscopy measurements was 400 nm.

In the emission spectra, **HBC-NMI** revealed peaks at ~480 and ~500 nm in toluene, which were red-shifted to ~550 nm in THF, due to the intramolecular CT (Figures 2B and S7).[14] Interestingly, **HBC-AQ** showed the emission maxima (λ_{em}) at ~560 nm in toluene with large Stokes shift of approximately 110 nm, based on the absorption maxima of the CT band at ~450 nm. The emission maxima of **HBC-AQ** further red-shifted to 680 nm when the solvent was changed to THF, corroborating the strong intramolecular donor-acceptor interactions in **HBC-AQ** (Figures 2B and S7). Additionally, **HBC-AQ** exhibited dual fluorescence

in THF with an emission peak at 492 nm from local excitation of the HBC moiety, in addition to the CT peak. This observation might be due to stabilization of different conformations of the molecule, depending on the solvent.[15] **HBC-PMI** displayed a small red-shift of emission peak (λ_{em}: 571 nm) from that of pristine **PMI** at ~550 nm (Figure 2B).[6b] The red-shift of the emission peak, comparing the spectra in toluene and THF, was also very limited (10 nm) (Figures S7), which provided further evidence for the weak intramolecular CT interactions between the **HBC** and **PMI** units. Among the three systems, **HBC-PMI** gave the highest quantum yield of 45% whereas **HBC-AQ** and **-NMI** exhibited that of around 8–9%. The optical energy gaps were estimated from the absorption onset in toluene to be 2.41 eV (**HBC-AQ**), 2.70 eV (**HBC-NMI**), and 2.16 eV (**HBC-PMI**), which demonstrated the possibility of fine-tuning the optical properties by changing the acceptor units.

Cyclic voltammetry (CV) analyses of the HBC-acceptor dyads were performed in THF with 0.1 M $Bu_4N^+PF_6^-$ electrolyte, an Ag reference electrode, and a platinum counter electrode, giving reversible reduction (Table 1 and Figure S5). The lowest unoccupied molecular orbitals (LUMO) energy levels were estimated from the onset of reduction and found to be shifted, depending on the attached acceptor units: –3.42, –3.31, and –3.51 eV for **HBC-AQ**, **-NMI**, and **-PMI**, respectively. The highest occupied molecular orbital (HOMO) energy levels could then be calculated using the estimated optical energy gaps to be –5.83, –6.01, and –5.67 eV for **HBC-AQ**, **-NMI**, and **-PMI**, respectively.

Density functional theory (DFT) calculations provided further insight into the CT interactions of the HBC-acceptor dyads, which disclosed that the LUMOs were generally distributed over the acceptor units whereas the HOMOs were distributed on the HBC unit (Figure 3). Especially, in the case of **HBC-AQ**, LUMO and HOMO were completely separated onto the acceptor (**AQ**) and donor (**HBC**) units, respectively, which suggested strong CT interactions. On the other hand, LUMO of **HBC-NMI** was partially extended to the HBC moiety. Moreover, the HOMO of **HBC-PMI** was moderately spread on to the **PMI** unit. These theoretical results were in agreement with experimental observation showing strong CT interactions in **HBC-AQ** and weaker interactions in **HBC-NMI** and **-PMI**. Additionally, the calculated dihedral angle (θ) between **HBC** and **AQ** units at the covalently attached bond was found to be 36°. The dihedral angles were similar for **HBC-NMI** and **-PMI** (~54°) due to the comparable steric demand (Table S2).

The influence of the different acceptor units on the supramolecular organization of the HBC-acceptor dyads was next investigated by differential scanning calorimetry (DSC) and two-dimensional wide-angle X-ray scattering (2D-WAXS) (Figure 4). The DSC scans of **HBC-AQ** and **-NMI** exhibited one phase transition between the crystalline and liquid crystalline phase at 82.2 and 96.7 °C, respectively (Figure 4A and S3). The slightly higher temperature for **HBC-NMI** was surprising, considering that the **NMI** unit possessed additional branched alkyl side chains, which were supposed to weaken the molecular interactions. In contrast to the observation of phase transitions for **HBC-AQ** and **-NMI**, **HBC-PMI** did not reveal any peak in the DSC measurement.

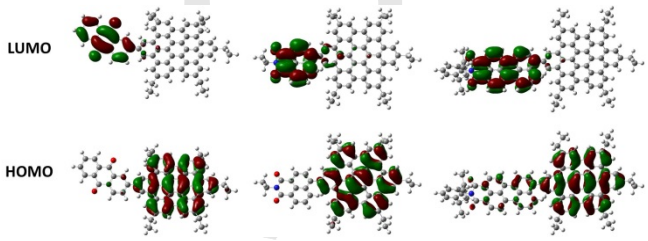

Figure 3. Calculated HOMOs and LUMOs of **HBC-AQ** (left), **-NMI** (middle), and **-PMI** (right) using DFT, B3LYP/6-31G (d).

Based on the DSC results, the supramolecular organization in bulk was investigated by using X-ray scattering. For these measurements, macroscopically aligned fiber samples were obtained through extrusion.[16] The scattering was collected by an area detector in the wide-angle range. As shown in Figure 4B and C, two typical 2D-WAXS patterns of **HBC-NMI** recorded at 120 and 30 °C, respectively, indicated its discotic LC columnar organization. In the LC phase, the disc-shaped molecules were packed on top of each other forming columnar structures (Figure 4B). The intracolumnar π-stacking distance of 0.35 nm was derived from meridional reflections, while the equatorial ones were attributed to the intercolumnar arrangement with stacks being oriented along the fiber axis. From the position of these scattering intensities a hexagonal unit cell with a parameter of a_{hex} = 2.94 nm was determined. Interestingly, **HBC-AQ** assembled in an identical hexagonal fashion, as the observation for **HBC-NMI**, in the LC phase (a_{hex} = 2.88 nm) (Figure 4). In the crystalline phase, **HBC-AQ** and **-NMI** organized also in similar supramolecular structures (Figure 4C and S4), where the columnar hexagonal organization was maintained with a slightly smaller a_{hex} parameter of 2.40 nm. In the stacks, the molecules displayed a herringbone tilting towards the columnar axis. In contrast to **HBC-AQ** and **-NMI**, **HBC-PMI** revealed solely a LC phase over the investigated temperature range without becoming crystalline (Figure 4D). The packing parameter was a_{hex} = 2.92 nm for the hexagonal unit cell and 0.35 nm for the π-stacking distance.

The supramolecular organization of the three HBC-acceptor dyads was quite surprising regarding the

Table 1. Photophysical and electrochemical properties of the HBC-acceptor dyads.

Compound	λ_{abs} (nm)[a]	λ_{em} (nm)[a]	Φ_F (%)[a]	E_{HOMO} (eV)[b]	$E_{LUMO,CV}$ (eV)[c]	$E_{g,opt}$ (eV)[d]
HBC-AQ	364; 392; 448	558	8.2	–5.83	–3.42	2.41
HBC-NMI	361; 394; 410; 450	482; 502	8.8	–6.01	–3.31	2.70
HBC-PMI	363; 392; 498; 523	571	45	–5.67	–3.51	2.16

[a] Absorption peaks (λ_{abs}), emission maxima (λ_{em}), and fluorescence quantum yields (Φ_F) were recorded in toluene. [b] HOMO level (E_{HOMO}) was calculated by $E_{HOMO} = E_{LUMO,CV} - E_{g,opt}$. [c] LUMO level ($E_{LUMO,CV}$) was determined by CV. [d] Optical energy gaps ($E_{g,opt}$) were estimated from the onset of the absorption spectra in toluene.

molecular design. One could expect that the substitution of the **HBC** disk with the bulky **AQ** or **NMI** units would result in a molecular rotation, e.g. in a helical fashion, due to the steric demand at the core periphery.[16a] Such a packing mode has been observed for HBC derivatives carrying an ethynyl bridged **PMI**.[8a] The thermotropic properties of **HBC-AQ** and **-NMI** were identical to the behavior of hexa-alkyl substituted HBC derivatives, indicating that the steric influence of the **AQ** and **NMI** units was negligible.[17] Attaching **PMI** did not disturb the packing of the **HBC-PMI** molecules as well, but suppressed their crystallinity, leading to a LC phase stable over a wide temperature range.

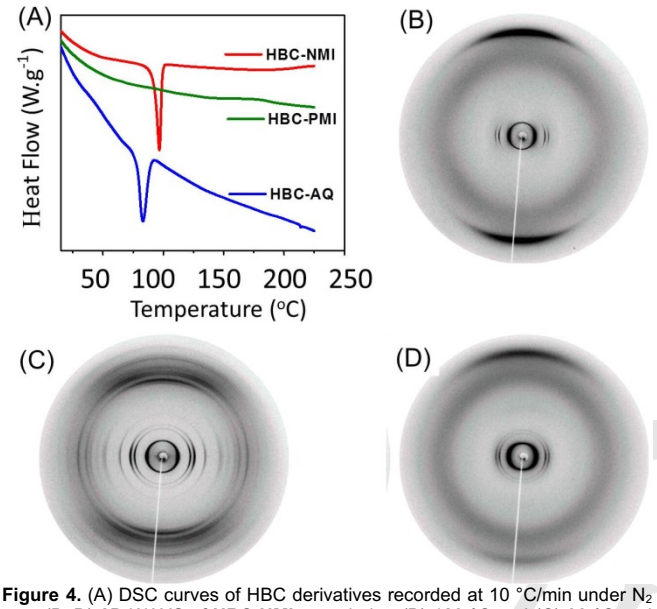

Figure 4. (A) DSC curves of HBC derivatives recorded at 10 °C/min under N_2 atm. (B–D) 2D-WAXS of **HBC-NMI** recorded at (B) 120 °C and (C) 30 °C and (D) **HBC-PMI** at 30 °C. The fiber samples were placed vertically in front of the detector.

In summary, three HBC-acceptor dyads, bearing 9,10-anthraquinone, naphthalene-1,8-dicarboximide, and perylene-3,4-dicarboximide units, were prepared through two synthetic routes, namely via the coupling of the acceptor unit before and after the cyclodehydrogenation of the HBC core. Photophysical, electrochemical, and liquid-crystalline properties of the HBC-acceptor dyads were studied, which demonstrated different degrees of intramolecular CT interactions and modulation of the energy gaps, depending on the acceptor units. These results marked the possibility of sensitively controlling the optoelectronic properties of such nanographene molecules through coupling with different acceptor units. Furthermore, the reported synthetic protocols can now be applied to larger nanographene molecules and graphene nanoribbons, paving the way towards new generation of nanographene-acceptor systems.

Experimental Section

All the experimental and theoretical details are provided in the Supporting Information.

Acknowledgements

We are grateful for the financial support from DFG Priority Program SPP 1459, Graphene Flagship (No. CNECT-ICT-604391), and European Community through the FET-Proactive Project “MoQuaS” (No. 610449) and Marie-Curie ITN project “iSwitch” (GA No. 642196). We greatly appreciate Klaus Müllen for valuable discussion and comments on the manuscript. We thank Sebastian Stappert for his kind help in the preparation of **PMI-boro**.

Keywords: donor–acceptor systems • nanographene • dehydrogenation • polycycles • charge transfer

[1] a) A. Narita, X.-Y. Wang, X. Feng, K. Müllen, *Chem. Soc. Rev.* **2015**, *44*, 6616-6643; b) J. Wu, W. Pisula, K. Müllen, *Chem. Rev.* **2007**, *107*, 718-747; c) X. Li, M. Rui, J. Song, Z. Shen, H. Zeng, *Adv. Funct. Mater.* **2015**, *25*, 4929-4947; d) K. P. Loh, S. W. Tong, J. Wu, *J. Am. Chem. Soc.* **2016**, *138*, 1095-1102; e) C. Soldano, A. Mahmood, E. Dujardin, *Carbon* **2010**, *48*, 2127-2150; f) Y. Segawa, H. Ito, K. Itami, *Nat. Rev. Mater.* **2016**, *1*, 15002.

[2] X. Yan, B. Li, L.-s. Li, *Acc. Chem. Res.* **2013**, *46*, 2254-2262.

[3] a) A. Narita, X. Feng, Y. Hernandez, S. A. Jensen, M. Bonn, H. Yang, I. A. Verzhbitskiy, C. Casiraghi, M. R. Hansen, A. H. R. Koch, G. Fytas, O. Ivasenko, B. Li, K. S. Mali, T. Balandina, S. Mahesh, S. De Feyter, K. Müllen, *Nature Chem.* **2014**, *6*, 126-132; b) T. H. Vo, M. Shekhirev, D. A. Kunkel, M. D. Morton, E. Berglund, L. Kong, P. M. Wilson, P. A. Dowben, A. Enders, A. Sinitskii, *Nat. Commun.* **2014**, *5*, 3189.

[4] a) X.-Y. Wang, J.-Y. Wang, J. Pei, *Chem.—Eur. J.* **2015**, *21*, 3528-3539; b) W. Jiang, Y. Li, Z. Wang, *Chem. Soc. Rev.* **2013**, *42*, 6113-6127; c) J. L. Segura, R. Juarez, M. Ramos, C. Seoane, *Chem. Soc. Rev.* **2015**, *44*, 6850-6885; d) M. Ball, Y. Zhong, Y. Wu, C. Schenck, F. Ng, M. Steigerwald, S. Xiao, C. Nuckolls, *Acc. Chem. Res.* **2015**, *48*, 267-276.

[5] a) Y.-Z. Tan, S. Osella, Y. Liu, B. Yang, D. Beljonne, X. Feng, K. Müllen, *Angew. Chem. Int. Ed.* **2015**, *54*, 2927-2931; b) R. Yamaguchi, S. Ito, B. S. Lee, S. Hiroto, D. Kim, H. Shinokubo, *Chem. Asian J.* **2013**, *8*, 178-190; c) W. W. H. Wong, J. Subbiah, S. R. Puniredd, B. Purushothaman, W. Pisula, N. Kirby, K. Müllen, D. J. Jones, A. B. Holmes, *J. Mater. Chem.* **2012**, *22*, 21131-21137; d) D. Lungerich, J. F. Hitzenberger, M. Marcia, F. Hampel, T. Drewello, N. Jux, *Angew. Chem. Int. Ed.* **2014**, *53*, 12231-12235; e) J. P. Hill, W. Jin, A. Kosaka, T. Fukushima, H. Ichihara, T. Shimomura, K. Ito, T. Hashizume, N. Ishii, T. Aida, *Science* **2004**, *304*, 1481-1483; f) S. Ito, M. Wehmeier, J. D. Brand, C. Kübel, R. Epsch, J. P. Rabe, K. Müllen, *Chem.–Eur. J.* **2000**, *6*, 4327-4342.

[6] a) F. Hinkel, D. Cho, W. Pisula, M. Baumgarten, K. Müllen, *Chem.—Eur. J.* **2015**, *21*, 86-90; b) L. F. Dössel, V. Kamm, I. A. Howard, F. Laquai, W. Pisula, X. Feng, C. Li, M. Takase, T. Kudernac, S. De Feyter, K. Müllen, *J. Am. Chem. Soc.* **2012**, *134*, 5876-5886; c) P. Samorì, A. Fechtenkötter, E. Reuther, M. D. Watson, N. Severin, K. Müllen, J. P. Rabe, *Adv. Mater.* **2006**, *18*, 1317-1321; d) W. W. H. Wong, J. Subbiah, S. R. Puniredd, B. Purushothaman, W. Pisula, N. Kirby, K. Mullen, D. J. Jones, A. B. Holmes, *J. Mater. Chem.* **2012**, *22*, 21131-21137; e) S. Ren, C. Yan, D. Vak, D. J. Jones, A. B. Holmes, W. W. H. Wong, *Adv. Funct. Mater.* **2012**, *22*, 2015-2026.

[7] a) J. L. Li, M. Kastler, W. Pisula, J. W. F. Robertson, D. Wasserfallen, A. C. Grimsdale, J. S. Wu, K. Müllen, *Adv. Funct. Mater.* **2007**, *17*, 2528-2533; b) T. Haßheider, S. A. Benning, M. W. Lauhof, H. S. Kitzerow, H. Bock, M. D. Watson, K. Müllen, *Molecular Crystals and Liquid Crystals* **2004**, *413*, 461-472.

[8] a) J. M. Mativetsky, M. Kastler, R. C. Savage, D. Gentilini, M. Palma, W. Pisula, K. Müllen, P. Samorì, *Adv. Funct. Mater.* **2009**, *19*, 2486-2494; b) Y. Yamamoto, W. Jin, T. Fukushima, T. Minari, K. Tsukagoshi, A. Saeki, S. Seki, S. Tagawa, T. Aida, *Chem. Lett.* **2009**, *38*, 888-889; c) A.

M. v. d. Craats, J. M. Warman, A. Fechtenkötter, J. D. Brand, M. A. Harbison, K. Müllen, *Avd. Mater.* **1999**, *11*, 1469-1472.

[9] P. Samorì, X. Yin, N. Tchebotareva, Z. Wang, T. Pakula, F. Jäckel, M. D. Watson, A. Venturini, K. Müllen, J. P. Rabe, *J. Am. Chem. Soc.* **2004**, *126*, 3567-3575.

[10] J. E. Bullock, M. T. Vagnini, C. Ramanan, D. T. Co, T. M. Wilson, J. W. Dicke, T. J. Marks, M. R. Wasielewski, *J. Phys. Chem. B* **2010**, *114*, 1794-1802.

[11] A. Keerthi, Y. Liu, Q. Wang, S. Valiyaveettil, *Chem. Eur. J.* **2012**, *18*, 11669-11676.

[12] S. Stappert, C. Li, K. Müllen, T. Basché, *Chem. Mater.* **2016**, *28*, 906-914.

[13] R. Rieger, K. Müllen, *J. Phys. Org. Chem.* **2010**, *23*, 315-325.

[14] G.-J. Zhao, R.-K. Chen, M.-T. Sun, J.-Y. Liu, G.-Y. Li, Y.-L. Gao, K.-L. Han, X.-C. Yang, L. Sun, *Chem.—Eur. J.* **2008**, *14*, 6935-6947.

[15] V. Thiagarajan, C. Selvaraju, E. J. P. Malar, P. Ramamurthy, *ChemPhysChem* **2004**, *5*, 1200-1209.

[16] a) W. Pisula, Ž. Tomović, M. D. Watson, K. Müllen, J. Kussmann, C. Ochsenfeld, T. Metzroth, J. Gauss, *J. Phys. Chem. B* **2007**, *111*, 7481-7487; b) M. R. Hansen, T. Schnitzler, W. Pisula, R. Graf, K. Müllen, H. W. Spiess, *Angew. Chem. Int. Ed.* **2009**, *48*, 4621-4624.

[17] W. Pisula, X. Feng, K. Müllen, *Avd. Mater.* **2010**, *22*, 3634-3649.

Entry for the Table of Contents (Please choose one layout)

Layout 1:

COMMUNICATION

Hexa-*peri*-hexabenzocoronene (HBC)-based donor-acceptor dyads were synthesized with three different acceptor units, 9,10-anthraquinone (**AQ**), naphthalene-1,8-dicarboximide (**NMI**), and perylene-3,4-dicarboximide (**PMI**). The three HBC-acceptor dyads demonstrated varying degrees of intramolecular charge-transfer interactions, allowing tuning of their photophysical and optoelectronic properties.

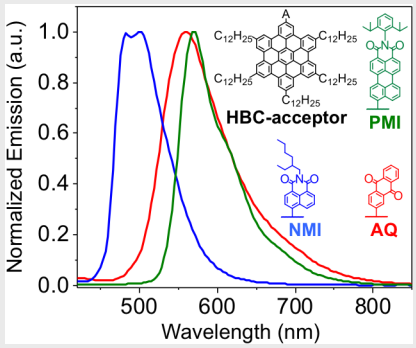

*Ashok Keerthi, Ian Cheng-Yi Hou, Tomasz Marszalek, Wojciech Pisula, Martin Baumgarten, and Akimitsu Narita**

Page No. – Page No.

Hexa-*peri*-hexabenzocoronene with Different Acceptor Units for Tuning Optoelectronic Properties

Layout 2:

COMMUNICATION

*Author(s), Corresponding Author(s)**

Page No. – Page No.

Title

Text for Table of Contents